Dynamics of a shear-induced aggregation process by a combined Monte Carlo-Stokesian Dynamics approach

Dynamics of a shear-induced aggregation process by a combined Monte Carlo-Stokesian Dynamics approach

Graziano Frungieri[1] **and Marco Vanni**[2]

[1]*Department of Applied Science and Technology, Politecnico di Torino*
Corso Duca degli Abruzzi, 24, 10129, Torino
graziano.frungieri@polito.it

[2]*Department of Applied Science and Technology, Politecnico di Torino*
Corso Duca degli Abruzzi, 24, 10129, Torino
marco.vanni@polito.it

Abstract

In the present work we investigated the collision efficiency of colloidal aggregates suspended in a shear flow. A Discrete Element Method (DEM), built in the framework of Stokesian Dynamics, was developed to model hydrodynamic and colloidal interactions acting on each primary particle composing the aggregates. Aggregates with complex geometries were generated by means of a combined DEM-Monte Carlo algorithm able to reproduce a shear-induced aggregation process occurring in a dilute colloidal suspension. Simulations, involving pairs of aggregates, were conducted according to a grid-based technique, in order to evaluate collision efficiencies. Size disproportion between aggregates and morphology shape anisotropy emerged as the principal causes affecting collision efficiencies. This work constitutes a first attempt to extend the traditional Von Smoluchowski's theory of shear-induced coagulation of spherical particles to the case of randomly-structured aggregates.

Keywords: Colloid aggregates, shear aggregation, collision efficiency, stokesian dynamics, shape anisotropy

1. Introduction

Suspensions of colloidal particles in low Reynolds number flows are relevant to a wide variety of engineering applications, including materials and food processing, water treatments, crystallization. In particular, the aggregation phenomena involving colloidal particles may have important consequences on the rheological properties of such suspensions as well as on their sedimentation behaviour.

The aggregation process can be activated by several mechanism such as Brownian motion, which is the prevailing mechanism for sub-micron particles suspended in low Péclet number flows, differential settling, which is relevant for larger particles characterized by a density significantly larger than that of the suspending fluid, or by spatial gradient of the velocity of the fluid. This latter mechanism, often referred to as *orthokinetic aggregation*, is by far the prevailing cause of aggregation in most of the application of practical interest, where the suspension is mechanically stirred. The simplest case of a spatially varying velocity field is a uniform shear flow. Hence, shear flows have been frequently used to investigate orthokinetic aggregation of colloidal particles. In fact, they can be easily reproduced with a lab equipment and offer a simple mathematical formulation, suitable for theoretical studies. Moreover it has been reported that a good correspondence exists between the aggregation conducted in a shear flow and the aggregation occurring in turbulent flows [1].

The first study about aggregation in a shear flow goes back to the work of Von Smoluchowski [2], who derived an expression for the rate of coagulation of spherical colloidal particles by assuming that the particles follow passively the streamlines of the undisturbed fluid flow. The effect of the hydrodynamic interaction among particles was addressed by several authors [4, 5, 6], who reviewed the classic Smoluchowski's theory of shear-induced coagulation introducing collision efficiency factors. However, all these studies dealt with spherical particles and the results cannot be extended straightforwardly to the case of randomly-structured aggregates, which are usually present in colloidal suspensions. Differently from the case of the collision of spherical particles, which is influenced mainly by the hydrodynamic and colloidal interactions, the study of the aggregation of irregular clusters is complicated by some additional factors such as orientation, shape and morphology.

The present work aims to investigate the collision efficiency in shear flow of irregular assemblies of equal spherical primary particles. To this purpose a Discrete Element Method, built in the framework of Stokesian Dynamics, was developed; Stokesian Dynamics is a well-established technique, which is able to model accurately hydrodynamic interactions between primary particles; coupling it with proper models to describe colloidal interactions, allowed us to explicitly take into account the irregular structure of aggregates without any simplifying assumption. A grid-based technique was developed to address the computation of collision efficiencies.

2. Methodology

2.1. DEM model

Hydrodynamic Interaction. Colloidal aggregates are assemblies of distinct elements, usually referred to as primary particles or monomers. For the present work, a Discrete Element Method (DEM) was developed to track the motion of each primary particle composing an aggregate, starting from the knowledge of the relevant forces and torques acting on it. The DEM model was built in the framework of Stokesian Dynamics [3]; based on the assumption that both the inertia of the primary particles and that of the fluid are negligible, Stokesian Dynamics relates the hydrodynamic force, torque and stresslet acting on the primary particles to their relative velocity with respect to the surrounding medium.

For a simple shear flow field of the kind $\mathbf{u}^{\infty}(\mathbf{r}) = \dot{\gamma} y \mathbf{e}_z$, with $\mathbf{e}_z$ being the unit vector aligned to the z direction, the undisturbed velocity of the medium, in any point identified by the position vector $\mathbf{r}$, can be expressed as the superposition of a pure rotating flow field (with angular velocity $\boldsymbol{\omega}^{\infty}$) and a pure straining motion (with the deformation rate tensor given by E^{∞}):

$$\mathbf{u}^{\infty}(\mathbf{r}) = \boldsymbol{\omega}^{\infty} \times \mathbf{r} + \mathsf{E}^{\infty}\mathbf{r}, \tag{1}$$

where the only non-zero elements are $\omega_x^{\infty} = \dot{\gamma}/2$ and $E_{yz}^{\infty} = E_{zy}^{\infty} = \dot{\gamma}/2$. Denoting by $\mathbf{F}_H$, $\mathbf{T}_H$ and $\mathbf{S}_H$ respectively the hydrodynamic force, torque and stresslet exerted by the fluid on the N suspended particles, in order to obtain the velocities of each of them, Stokesian Dynamics requires the solution of a linear system of the following kind:

$$\begin{bmatrix} R^{UF} & R^{\omega F} & R^{EF} \\ R^{UT} & R^{\omega T} & R^{ET} \\ R^{US} & R^{\omega S} & R^{ES} \end{bmatrix} \begin{Bmatrix} \mathbf{u}^{(1)} - \mathbf{u}^{\infty}(\mathbf{r}_1) \\ \vdots \\ \mathbf{u}^{(N)} - \mathbf{u}^{\infty}(\mathbf{r}_N) \\ \boldsymbol{\omega}^{(1)} - \boldsymbol{\omega}^{\infty} \\ \vdots \\ \boldsymbol{\omega}^{(N)} - \boldsymbol{\omega}^{\infty} \\ -\mathsf{E}^{\infty} \\ \vdots \\ -\mathsf{E}^{\infty} \end{Bmatrix} = \begin{Bmatrix} \mathbf{F}_H^{(1)} \\ \vdots \\ \mathbf{F}_H^{(N)} \\ \mathbf{T}_H^{(1)} \\ \vdots \\ \mathbf{T}_H^{(N)} \\ \mathbf{S}_H^{(1)} \\ \vdots \\ \mathbf{S}_H^{(N)} \end{Bmatrix} \tag{2}$$

where $\mathbf{r}_1$, $\mathbf{r}_N$ are the vector pointing to the centre of mass of the suspended particles. The stresslet and the deformation rate tensor relative to each particle are reduced to 5 elements-vectors, taking advantage of the fact that they are both symmetric and traceless (the full description of the method can be found in Ref. [3]). The resistance matrix $\mathcal{R}$ has dimension $11N \times 11N$ and it is computed at each time-step on the basis of the positions of the monomers; it takes into account both the far-field effects and the near-field effects (i.e., lubrication phenomena) of the hydrodynamic interaction.

Under the assumption of negligible inertia, after a force and torque balance on each primary particle α $\left(\mathbf{F}_H^{(\alpha)} = \sum_k \mathbf{F}_{ext,k}^{(\alpha)}, \mathbf{T}_H^{(\alpha)} = \sum_k \mathbf{T}_{ext,k}^{(\alpha)}\right)$, the linear system of Eqn (2) can be conveniently rewritten in a more compact way as

$$\begin{bmatrix} R^{UF} & R^{\omega F} \\ R^{UT} & R^{\omega T} \end{bmatrix} \begin{Bmatrix} \mathbf{u} - \mathbf{u}^{\infty} \\ \boldsymbol{\omega} - \boldsymbol{\omega}^{\infty} \end{Bmatrix} = \begin{Bmatrix} \mathbf{F}_{ext} \\ \mathbf{T}_{ext} \end{Bmatrix} + \begin{Bmatrix} R^{EF} \cdot \mathsf{E}^{\infty} \\ R^{ET} \cdot \mathsf{E}^{\infty} \end{Bmatrix}, \tag{3}$$

where $\mathbf{F}_{ext}$ and $\mathbf{T}_{ext}$ are the vectors containing the external forces and torques, other than the hydrodynamic ones, arising from the colloidal interactions between primary particles. Introducing proper models for the estimation of these forces and torques, the only unknown variables in Eqn (3) are the linear and angular velocities of the particles ($\mathbf{u}$ and $\boldsymbol{\omega}$), from whose integration is possible to know the exact trajectory of each primary particle.

Colloidal Interaction. Both central and tangential colloidal interactions were assumed to act on the primary particles. Central forces are those acting along the centre-to-centre vector $\mathbf{r}_{\alpha\beta} = |\mathbf{r}_{\alpha} - \mathbf{r}_{\beta}|$, with $\mathbf{r}_{\alpha}$ and $\mathbf{r}_{\beta}$ being the vectors pointing to the centres of particles α and β in a $Oxyz$ reference system. These forces act on the particles whether they are bonded or not to others and stem either from Van der Waals interactions or from contact interactions. Electrical double layer interactions are usually assumed to act along the centre-to-centre vector, as well; however they were not considered for the present work. Tangential forces are instead those forces acting on a couple of bonded particles, along the contact plane in such a way to prevent sliding and rolling, and are usually generated by friction.

When the separation distance h between the surfaces of two particles falls below 20 nm the Van der Waals attraction begins to be relevant. The resulting force was modelled according to

$$F_{vdw} = \frac{A_H \cdot a}{12 \cdot (h + z_0)^2} \cdot f(h) \tag{4}$$

where A_H is the Hamaker constant, a is the common primary particle radius and z_0 is the minimum approach distance, assumed equal to 1.65 Å; for large separation distances retardation effects are significant and responsible for a reduction of the interaction intensity; these effect were modelled by means of a coefficient $f(h) < 1$ according to Ref. [5].

Once a contact between the surface of two primary particles was established the mechanical response of the bond was modelled resorting to the JKR theory [7]. Given the adhesion force $F_{adh} = (3/2)\pi\gamma_s a$, with $\gamma_s = A_H / \left(24\pi z_0^2\right)$ being the surface energy of the solid, an approximate relation between the force acting on the particles and surface-to-surface distance was employed

$$F_{JKR} = F_{adh}\left[-1 + 1.1 \cdot \left(\tilde{h} - \tilde{h}_{po}\right)^{5/3}\right] \tag{5}$$

where the surface-to-surface distance is adimensionalized as $\tilde{h} = ha/b_0^2$ and the adimensionalized pull-off distance is given by:

$$\tilde{h}_{po} = \frac{a}{b_0^2}\left(\frac{3\pi^2\gamma_s^2 a\left(1-\nu^2\right)^2}{8E^2}\right)^{1/3} \tag{6}$$

where ν and E are respectively the Poisson ratio and the elastic modulus and b_0 is the zero-load contact radius given by $b_0 = \left(9\pi\gamma_s a^2\left(1-\nu^2\right)/2E\right)^{1/3}$. The force in Eqn (5), as the one of Eqn (4), was assumed to act along the centre-to-centre vector $\mathbf{r}_{\alpha\beta}$. Their combination provides the bond between two particles with a tensile strength.

However, as recently shown by Pantina and Furst [9] the large adhesion interaction between two bonded colloidal particles, is able to also hinder the relative displacement along the contact plane. Therefore, a spring-like model to confer a torsional, rolling and sliding resistance to a bond between two particles was adopted [10]. With regard to Fig. 1, two springs were ideally initialized when two particles came into mechanical contact.

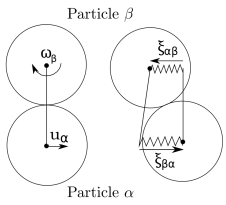

Figure 1: Representation of the spring-like force model proposed by Becker and Briesen [10]

Denoting by $\xi_{\alpha,\beta}$ and $\xi_{\beta,\alpha}$ the elongation of the springs induced by the relative tangential velocity, the restoring forces were computed as

$$\mathbf{F}_{\alpha} = k_t\left(\boldsymbol{\xi}_{\alpha,\beta} - \boldsymbol{\xi}_{\beta,\alpha}\right) \qquad \mathbf{F}_{\beta} = k_t\left(\boldsymbol{\xi}_{\beta,\alpha} - \boldsymbol{\xi}_{\alpha,\beta}\right) \tag{7}$$

while the corresponding torques as

$$\mathbf{T}_{\alpha} = 2ak_t\mathbf{r}_{\alpha,\beta} \times \boldsymbol{\xi}_{\alpha,\beta} \qquad \mathbf{T}_{\beta} = -2ak_t\mathbf{r}_{\beta,\alpha} \times \boldsymbol{\xi}_{\beta,\alpha} \tag{8}$$

where k_t is the stiffness of the springs. In a similar fashion, a thought torsional spring was also introduced when two particles

got in contact. Denoting by $\phi_{\alpha,\beta}$ the torsion angle of the spring, the restoring torque was set equal to

$$\mathbf{T}_\alpha = -\mathbf{T}_\beta = k_\phi \phi_{\alpha,\beta} \mathbf{r}_{\alpha,\beta} \tag{9}$$

The torsional stiffness k_ϕ and the tangential stiffness k_t as well as the corresponding maximal spring elongations ϕ_{max} and ξ_{max} were estimated as outlined in Ref. [9, 10].

2.2. *Aggregate generation*

Aggregates were generated using the DEM model together with a Monte Carlo algorithm capable of reproducing a particular realization of a shear-induced aggregation process. The Monte Carlo algorithm was based on the aggregation kernel drawn by Von Smoluchowski [2] for a dilute suspension of spherical particles

$$k_{i,j} = \frac{4}{3}\dot{\gamma}\left(a_i + a_j\right)^3 \tag{10}$$

with $\dot{\gamma}$ being the shear rate, and a_i, a_j being the radii of the two particles involved in a binary aggregation event. Since in this work we dealt with irregular assemblies of primary particles the aggregation kernel of Eqn (10) was reformulated replacing a_i and a_j with $R_{out,i}$ and $R_{out,j}$, the outer radii of the aggregates (i.e., the radius of the smallest sphere encompassing the aggregate). Thus, starting from an extremely dilute suspension of primary particles (volumic solid fraction $= 10^{-4}$), the Monte Carlo algorithm was used to sample a sequence of distinct and separated in time binary aggregation events between the suspended aggregates [8], while accurate reproduction of each event was obtained by the DEM model. Table 1 reports the main parameters of the DEM simulations. The system considered is composed by neutrally buoyant polystyrene particles suspended in water.

Table 1: Input parameters of the DEM simulations

Parameter	Symbol	Value
Hamaker constant	A_H	$0.97 \cdot 10^{-20}$ J
Particle radius	a	500 nm
Particle and medium density	ρ	1000 kg m^{-3}
Medium viscosity	η	10^{-3} Pa s
Shear rate	$\dot{\gamma}$	10 s^{-1}
Elastic modulus	E	3.4 GPa
Poisson ratio	ν	0.3
Minimum approach distance	z_0	0.165 nm
Time-step length	Δt	10^{-7} s
Tangential spring stiffness	k_t	$1.85 \cdot 10^{-5}$ N m^{-1}
Torsional spring stiffness	k_ϕ	$9.2 \cdot 10^{-9}$ nN m/rad
Maximal spring elongation	ξ_{max}	50 nm
Maximal spring torsion	ϕ_{max}	0.10 rad

2.3. *Evaluation of the aggregation efficiency*

Using the clusters generated by the shear-induced aggregation process, a detailed study of the aggregation efficiencies was carried out according to a grid-based technique.

The collision efficiencies were evaluated in the shear flow $\mathbf{u}^\infty(\mathbf{r}) = \dot{\gamma} y \mathbf{e}_z$ (Fig. 2). Given a pair of aggregates i,j with outer radius respectively $R_{out,i}$ and $R_{out,j}$, a 20×20 evenly spaced quadrilateral mesh was generated in a plane $z = -5 \cdot (R_{out,i} + R_{out,j})$ within the quadrant $y > 0$, $x > 0$. The size of each side of the mesh was set equal to $R_{out,i} + R_{out,j}$. At the beginning of each simulation the centre of mass of the aggregate j was placed on a node of the mesh.

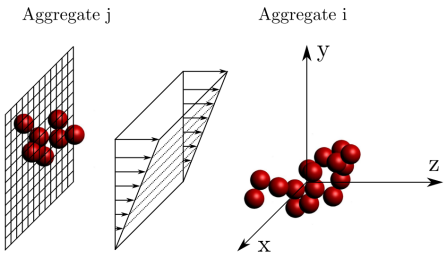

Figure 2: Initial configuration of an encounter event between aggregate j, composed by 8 primary particles, and aggregate i, made of 16 primary particles.

The aggregate i was placed instead in the origin of the reference system. From this initial configuration the DEM model was used to track the motion of both aggregates and to ascertain the outcome of the event, which can result in:

- an aggregation,
- a missed aggregation

In the first case, the two aggregates collide and generate a new larger aggregate. In the second case, the aggregate j pass close to the aggregate i without colliding with it. In order to save computational costs, for both cases a stop criterion was adopted: in the aggregation case, the simulation was stopped once a mechanical contact between the two involved aggregates was established; this choice is justified by the fact that, due to the deep potential well, aggregates coagulate irreversibly once two of their constituent primary particles touch; restructuring phenomena are beyond the scope of the present work. For missed collisions a different criterion was adopted; once the aggregate j passed over the aggregate i, simulation was stopped when the distance between the centres of mass of the aggregates along the z-direction exceeded a threshold value set equal to $2 \cdot (R_{out,i} + R_{out,j})$. In order to infer statistical reliable informations, for each node of the mesh, every encounter event was repeated 4 times, changing each time the initial orientation of both aggregates in the flow field.

3. Results and discussion

The aim of the present work was the determination of the aggregation efficiencies for irregular assemblies of colloidal particles. As previously mentioned, an encounter between a pair of aggregates may or not result into an aggregation event. Several synergistic effects come into play when aggregates move towards each other, such as Van der Waals attraction, long-ranged hydrodynamic interactions, lubrication forces. They strongly depend on morphology, orientation and size of both aggregates. All these aspects are easily addressed by the DEM model adopted.

Following the previously outlined grid-based technique, several collision maps were obtained. As an example, Fig. 3 reports the one relative to a pair of aggregates composed respectively by 6 and 5 primary particles. Each node of the mesh is indicated as black dot; the shade intensity of the cells is a measure of the fraction of repetitions ended into a successful aggregation.

The evaluation of the aggregation efficiency was conducted by comparing the flow rate of particles crossing the shaded collision section with the flow rate crossing the collision section assumed by the model of Von Smoluchowski, circumscribed by a solid curve in Fig. 3.

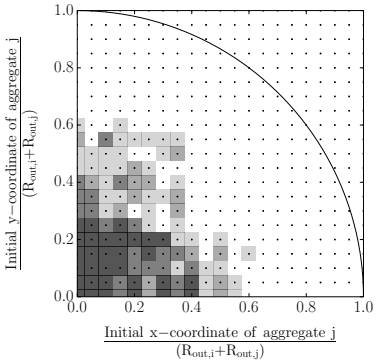

Figure 3: Collision cross section relative to a pair i,j of aggregates. Aggregate i is composed by 6 primary particles with an outer radius equal to 1.7 μm. Aggregate j is composed by 5 primary particle with an outer radius equal to 1.95 μm

Therefore the collision efficiency $\alpha_{i,j}$ relative to a pair of aggregates i and j reads as

$$\alpha_{i,j} = \frac{\int_{S_{\mathrm{sh}}} \dot{\gamma} y \cdot \omega\left(x,y\right) dS}{\int_{S_{\mathrm{Smol}}} \dot{\gamma} y dS} \tag{11}$$

where the integral at the numerator is extended to the whole shaded region. The weight function $\omega\left(x,y\right)$ quantifies the fraction of successful aggregation ($= 1/4, 2/4, 3/4$ or $4/4$) occurred for an initial position of the aggregate j.

3.1. Particle-Cluster aggregation

An aggregation event involving a primary particle and an aggregate is usually referred to as *Particle-Cluster Aggregation* (PCA). In the present work this phenomenon was investigated conducting several simulations involving a primary particle and various aggregates, differing essentially in the number of constituent primary particles.

Particle-particle aggregation can be considered a specific subcase of PCA, particularly relevant in the initial phase of any aggregation process. To study this phenomenon, the grid-based approach outlined earlier was employed with the only obvious modification in the number of repetitions performed; because of the spherical symmetry of both particles, it is sufficient to execute one repetition for each node of the mesh. Figure 4a reports the trajectories followed by a monomer j, relatively to a monomer i, in the shear flow for different starting y-coordinate of the monomer j. The plot illustrates solely the trajectories which led to a missed collision. As apparent, our model addressed properly the effect of the hydrodynamic interactions on the particle trajectories. Due to these interactions, the trajectory of the particle j is more and more deflected from the rectilinear streamlines as it approaches the central particle i. This effect acts preventing the collision and the formation of a doublet, even if the the initial position of the particle j fell in the collision section hypothesised in Von Smoluchowski's analysis. As a measure of the deflection entity, the difference between the maximum y-coordinate reached during the motion, $\max\left(y_1\left(t\right)\right)$, and the initial y-coordinate $y_1\left(t=0\right)$ was computed. Figure 4b reports this quantity as a function of the initial y-coordinate of the j primary particle. As predictable, as the initial y-coordinate increases, the disturb the particle j perceives is diminished; the quantity used to measure deflection was found to follow precisely a decay law of the kind $y_0^{-2.7}$.

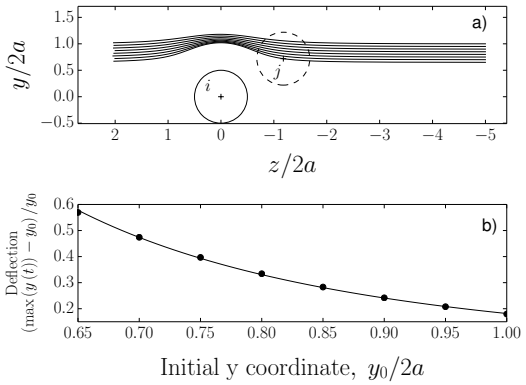

Figure 4: a) Relative trajectory of a primary particle j for different initial y-coordinate. The x-coordinate is zero for all cases. b) The amount of deflection as a function of the initial y-coordinate of the particle j.

When moving to irregular assemblies of spherical primary particles, orientation is a crucial issue. As already mentioned, this aspect was addressed changing time by time the initial orientation of the aggregate. Despite the relatively low number of repetitions, this strategy allowed us to uncouple efficiently the computed efficiencies from the relative orientations. Figure 5 reports the collision efficiencies $\alpha_{i,1}$ relative to a primary particle and an aggregate i as a function of their mass ratio m_i/m_1.

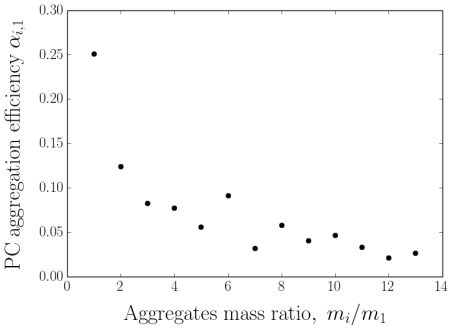

Figure 5: Particle-Cluster aggregation efficiency as a function of the relative mass.

It is evident that, as the size difference between the involved aggregates increases, a reduction in the collision efficiency appears. This phenomenon can be interpreted in the light of a magnified hydrodynamic solicitation acting on the approaching primary particle, when the aggregate i grows in size. Hydrodynamic interactions are in fact modelled in a pair-wise additivity manner in Stokesian Dynamics. Therefore it is clear that the larger the number of primary particle composing the i aggregate is, the more intense is the disturb induced in the surrounding medium. As a consequence, the approaching primary particle, given its relatively small inertia, is substantially deviated from its trajectory. Analogously to Fig. 4b, Fig. 6 reports the deflection of the trajectory of the primary particle computed as the difference between the maximum y-coordinate reached during the motion $\max\left(y_1\left(t\right)\right)$ and the initial y-coordinate $y_1\left(t=0\right)$, normalized by the primary particle radius a. To infer statistical reliable data, an average extended to all the events, which turned into a missed collision, was performed.

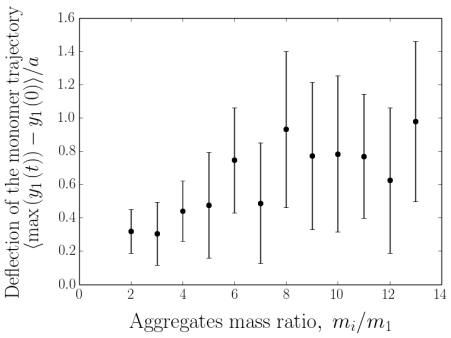

Figure 6: Average deflection of the primary particle trajectory as a function of the aggregates mass ratio. The average is extended to all the encounter events which turned into a missed collision. Error bars indicate the standard deviation of the data.

As apparent, the trajectory of the monomer is more substantially deviated from the rectilinear streamlines of the flow field, as the size of the i aggregate increases. It is worth to point out that the wide scatter of the data has not to be regarded as an uncertainty affecting the results, but rather as a consequence of the initial y coordinate of the primary particle. As shown earlier in Fig. 4b, the release point of the j primary particle has a strong influence on the entity of the deflection.

3.2. Cluster-Cluster Aggregation

When the aggregates involved in an encounter event are comparable in size, their morphologies play a central role; in particular, the shape anisotropy appeared to affect seriously aggregation efficiencies.

In order to quantify the shape anisotropy of the clusters, we translated their structure into their inertia-equivalent ellipsoid. First we computed the inertia tensor of each constituent solid primary particle α in a reference system centred in their centre of mass as $\mathbf{I}_{\alpha,ii} = 2/5 m_\alpha a^2$, with $m_\alpha = 4/3\pi\rho a^3$ being their mass. Subsequently, in order to obtain the inertia tensor relative to the reference system centred in the centre of mass of the aggregate, we applied the parallel axis theorem in its tensorial formulation to the inertia tensor of each primary particle α as

$$\mathbf{I}'_\alpha = \mathbf{I}_\alpha + m_\alpha \left(|\mathbf{r}_\alpha| \, \delta_{ij} - r_{\alpha,i} r_{\alpha,j} \right) \tag{12}$$

with $\mathbf{r}_\alpha$ being the vector directed from the center of mass of the cluster to the centre of mass of the particle α and δ_{ij} being the Kronecker delta. Consequently the inertia tensor of the cluster was obtained as

$$\mathbf{I}_{cluster} = \sum_\alpha \mathbf{I}'_\alpha \tag{13}$$

The principal moments of inertia ($I_1 > I_2 > I_3$) of the cluster were obtained by diagonalizing $\mathbf{I}_{cluster}$ and the length of the principal semi-axes ($a_1 > a_2 > a_3$) as:

$$\begin{aligned} a_1 &= \sqrt{\frac{5}{2} \frac{I_2 + I_3 - I_1}{\sum_\alpha m_\alpha}} \\ a_2 &= \sqrt{\frac{5}{2} \frac{I_1 + I_3 - I_2}{\sum_\alpha m_\alpha}} \\ a_3 &= \sqrt{\frac{5}{2} \frac{I_1 + I_2 - I_3}{\sum_\alpha m_\alpha}} \end{aligned} \tag{14}$$

Therefore the shape anisotropy ($S.A.$) of each aggregate was estimated as:

$$\text{S.A.} = \frac{2a_1}{a_2 + a_3} > 1 \tag{15}$$

Equation (15) returns values close to 1 for round-shaped aggregates and substantially larger values for the rod-shaped ones.

The shape anisotropy has profound implications on the aggregate motion. Perfectly spherical particles (S.A.=1) in a shear flow $\mathbf{u}^\infty(\mathbf{r}) = \dot{\gamma} y \mathbf{e}_z$ rotate with constant angular velocity ($\omega_x = \dot{\gamma}/2$); on the contrary, randomly structured clusters exhibit a more complex motion.

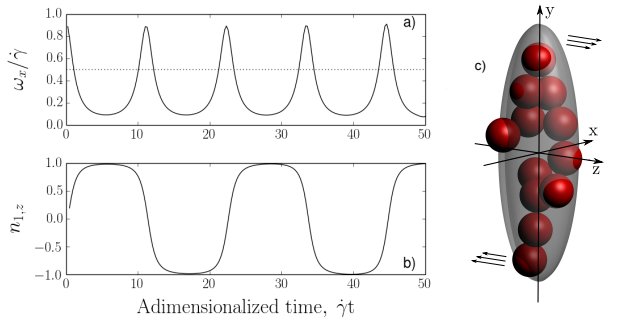

Figure 7: Motion of a rod-shaped aggregate (shape anisotropy=3.33) composed by 12 primary particles suspended in a shear flow $\mathbf{u}^\infty(\mathbf{r}) = \dot{\gamma} y \mathbf{e}_z$. a) Time dependence of the x-component of the angular velocity (solid curve). The dotted line represents the angular velocity of a perfectly spherical particle. b) Time dependence of the z-component of the principal inertia axis unit vector, $n_{1,z}$.

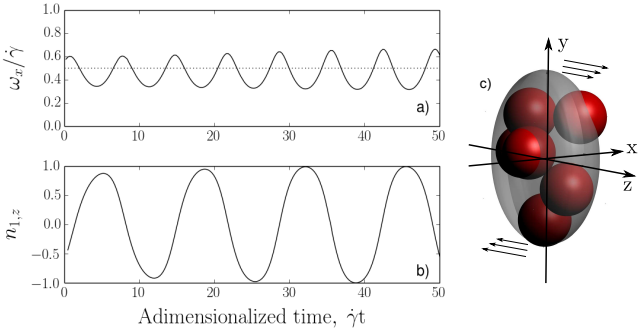

Figure 8: Motion of a round-shaped aggregate (shape anisotropy=1.54) composed by 6 primary particles suspended in a shear flow $\mathbf{u}^\infty(\mathbf{r}) = \dot{\gamma} y \mathbf{e}_z$. a) Time dependence of the x-component of the angular velocity (solid curve). The dotted line represents the angular velocity of a perfectly spherical particle. b) Time dependence of the z-component of the principal inertia axis unit vector, $n_{1,z}$.

Figures 7 and 8 report the time dependence of the x-component of the angular velocity of two aggregates, different one from the other in their shape anisotropy. For both aggregates the angular velocity shows a fluctuation around the average value ($\omega_x = \dot{\gamma}/2$), but the amplitude of the fluctuations differs

substantially in the two cases. For rod-shaped aggregates the velocity stays at its minimum value for a quite long time, during which the rotation is slow. The long duration of this phase has to be related to the reduced magnitude of the overall hydrodynamic torque acting on the aggregate. As apparent in Fig. 7b, this stage corresponds to the maximum alignment of the principal inertia axis with the flow direction (the z-direction in this particular case). Quite suddenly ω_x steeply increases to reach its maximum value. This peak occurs when the aggregate is orthogonal to zero-shear plane (Fig. 7c). In this situation the torque acting on the aggregate is at its maximum value and make the aggregate to rapidly rotate till it aligns again with the fluid velocity. The round-shaped aggregate depicted in Fig. 8 exhibits a scarcely similar behaviour: the angular velocity oscillates about the average value ($\omega_x = \dot{\gamma}/2$) as well, but oscillations are much smoother and characterized by a smaller amplitude. As it will be discussed soon, the different motion that round-shaped and rod-shaped aggregates exhibit in shear flow has profound implications on the collision efficiencies.

The plot in Fig. 9 reports the collision efficiencies computed for different pairs of aggregate i,j; the two aggregates depicted in Fig. 7c and Fig. 8c were used as central i aggregates, according to the set-up scheme of Fig. 2. Encounter simulations with several j aggregates, different in S.A., were performed. As apparent, whether the morphology of the i aggregate is, a noticeable reduction in the collision efficiency arises as the S.A. of the j aggregate grows. This effect is the direct result of the different motion of round-shaped and rod-shaped aggregates in shear flow. In fact round-shaped aggregates maintain during their motion an almost constant cross section; on the contrary, elongated ones exhibit a continuous change of their cross section, which oscillates continuously between its minimum and maximum value, with the former retained for a much longer period of time. This feature makes missed collision most likely to occur since the elongated aggregates have a much higher probability to pass over the i aggregate with their minimum cross section, thus without hitting the i central aggregate.

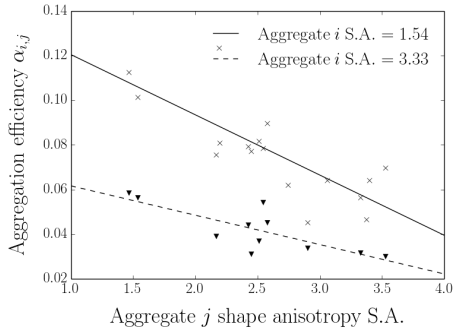

Figure 9: Cluster-cluster aggregation efficiency as a function of the shape anisotropy. The data reported are relative to aggregates composed by a number of primary particles ranging from 2 to 20.

Furthermore, it is evident from the plot that this argument holds with the increasing S.A. anisotropy of the i central aggregates, as well. In fact the collision efficiencies relative to the rod-shaped aggregate (S.A.=3.33) are all lower than the ones corresponding to the round-shaped aggregate (S.A.=1.54). It can be concluded that the shape anisotropy effects are magnified when both clusters involved in an encounter event present a rod-shaped morphology.

4. Conclusions

The collision efficiency of rigid aggregates with complex morphology suspended in a uniform shear flow was investigated. The aggregates were generated by means of a Monte Carlo-DEM algorithm able to reproduce a particular realization of a shear induced aggregation process. The aggregates, composed by equally sized spherical primary particles, covered a quite broad range of masses and shape anisotropies. To quantify collision efficiencies in shear flow a grid based technique was employed together with a DEM model. To the best of our knowledge such an approach has never been employed to address this task.

Our simulations highlighted that two main factors determine collision probabilities: for particle-cluster aggregation events, size disproportion appeared to strongly affect aggregation. Large aggregates were able in fact to substantially disturb the flow field and, as a consequence, to significantly deflect primary particle trajectories, thus preventing aggregation. Differently, in cluster-cluster encounters, shape anisotropy turned up to be the main factor affecting collision efficiencies. Large shape anisotropy has been linked, in fact, to significant reduction of the time-averaged collision cross section of the aggregates.

Results are encouraging and indicate our methodology as a valid approach to the determination of collision efficiencies between irregular clusters of colloidal particles. However further work is planned to expand the library of analysed clusters in order to state if the validity of our findings can be directly extended to larger aggregates. In perspective these results may lead to a precise correlation between morphologies and aggregation efficiency that can be useful to fine-tune Population Balance Equations for the shear-induced aggregation of colloidal particles.

References

[1] Kusters, K.A., Wijers, J.G. and Thoenes D., Aggregation kinetics of small particles in agitated vessels, *Chem. Eng. Sci.*, 52.1, pp. 107-121, 1997

[2] Smoluchowski Von, M., Versuch einer Mathematischen Theorie der Koagulationskinetic Kolloider LÃűsunger, *Z. Phys. Chem* 92, pp. 129-168, 1917

[3] Durlofsky, L., Brady, J.F. and Bossis G., Dynamic simulation of hydrodynamically interacting particles, *J. Fluid. Mech.*, 180, pp. 21-49, 1987.

[4] Higashitani, K. O., Ogawa, R., Hosokawa, G. and Matsuno, Y., Kinetic theory of shear coagulation for particles in a viscous fluid, *J. Chem. Eng. Jpn.*, 15, pp. 299-304, 1982.

[5] Vanni, M. and Baldi, G., Coagulation efficiency of colloidal particles in shear flow, *Adv. Colloid Interfac.*, 97, pp. 151-177, 2002.

[6] Arp, P.A. and Mason, S.G., Orthokinetic collisions of hard spheres in simple shear flow, *Can. J. Chem.*, 54 pp. 3769-3774, 1976.

[7] Johnson, K. L., Kendall, K. and Roberts A.D., Surface energy and the contact of elastic solids, *P. Roy. Soc. Lond. A. Mat.*, Vol. 32, pp. 301-313, 1971.

[8] Liffman, K., A direct simulation Monte-Carlo method for cluster coagulation, *J. Comput. Phys.*, 100, pp. 116-127, 1992.

[9] Pantina, J.P. and Furst, E.M., Elasticity and critical bending moment of model colloidal aggregates. *Phys. Rev. Lett.*, 94, pp. 138301.1-4, 2005.

[10] Becker, V. and Briesen, H., Tangential-force model for interactions between bonded colloidal particles. *Phys. Rev. E*, 78, pp. 061404.1-9, 2008.